

## BLUE SUPERGIANT MODEL FOR ULTRA-LONG GAMMA-RAY BURST WITH SUPERLUMINOUS-SUPERNOVA-LIKE BUMP

DAISUKE NAKAUCHI<sup>1</sup>, KAZUMI KASHIYAMA<sup>2</sup>, YUDAI SUWA<sup>3</sup>, AND TAKASHI NAKAMURA<sup>1</sup>

*Draft version November 14, 2021*

### ABSTRACT

Long GRBs (LGRBs) have typical duration of  $\sim 30$  s and some of them are associated with hypernovae, like Type Ic SN 1998bw. Wolf-Rayet stars are the most plausible LGRB progenitors, since the free-fall time of the envelope is consistent with the duration, and the natural outcome of the progenitor is a Type Ic SN. While a new population of ultra-long GRBs (ULGRBs), GRB 111209A, GRB 101225A, and GRB 121027A, has a duration of  $\sim 10^4$  s, two of them are accompanied by superluminous-supernova (SLSN) like bumps, which are  $\lesssim 10$  times brighter than typical hypernovae. Wolf-Rayet progenitors cannot explain ULGRBs because of too long duration and too bright SN-like bump. A blue supergiant (BSG) progenitor model, however, can explain the duration of ULGRBs. Moreover, SLSN-like bump can be attributed to the so-called cocoon-fireball photospheric emissions (CFPEs). Since a large cocoon is inevitably produced during the relativistic jet piercing through the BSG envelope, this component can be a smoking-gun evidence of BSG model for ULGRBs. In this paper, we examine u, g, r, i, and J-band light curves of three ULGRBs and demonstrate that they can be fitted quite well by our BSG model with the appropriate choices of the jet opening angle and the number density of the ambient gas. In addition, we predict that for 121027A, SLSN-like bump could have been observed for  $\sim 20$ -80 days after the burst. We also propose that some SLSNe might be CFPEs of off-axis ULGRBs without visible prompt emission.

*Subject headings:* gamma rays: bursts — gamma rays: observations — gamma rays: theory — gamma rays: individual (GRB 111209A, GRB 101225A, GRB 121027A)

### 1. INTRODUCTION

Long gamma-ray bursts (LGRBs), whose durations are longer than 2 s, are considered to originate from core collapses of massive stars (Woosley 1993; MacFadyen & Woosley 1999). In standard collapsar scenario, a relativistic jet launched from a central engine (a black-hole (BH) accretion disk or a magnetar) burrows through the progenitor, and finally punches out. Then the prompt gamma rays are produced by some dissipation processes in the jet, although the mechanism is still uncertain (see Mészáros 2013, for a recent review). So far, some LGRBs were associated with type Ic supernova (SN) (e.g., Hjorth & Bloom 2011; Zhang et al. 2012; Xu et al. 2013), which might imply that collapsars come from CO Wolf-Rayet (WR) stars. They are plausible progenitors from the theoretical point of view in that they have no hydrogen and helium envelopes, and thus jets can penetrate them more easily (Matzner 2003). Also, the typical observed duration of LGRBs,  $\sim 30$  s, is consistent with the accretion timescale of the WR progenitor envelope onto the central engine.

The above WR model could not be applied to recently discovered ultra-long GRBs (ULGRBs), GRB 101225A, GRB 111209A, and GRB 121027A (Gendre et al. 2013; Levan et al. 2013). They all have observed durations of  $\sim 10^4$  s, which are much longer than the anticipated cen-

tral engine lifetimes of CO WR collapsars. There were a few proposals in the literature for the *Christmas burst*, GRB 101225A, such as a tidal disruption of a comet by a galactic neutron star (Campana et al. 2011), or an extragalactic outburst triggered by a stellar merger in a neutron-star binary system at  $z = 0.33$  (Thöne et al. 2011). However, at least the former model is now unlikely in terms of the energetics after the redshifts of these bursts are determined;  $z = 0.847$  for GRB 101225,  $z = 0.677$  for GRB 111209A, and  $z = 1.773$  for GRB 121027A (Levan et al. 2013). Other possible non-collapsar-jet scenarios are SN shock breakouts (e.g., Campana et al. 2006), or tidal disruption of a star by the supermassive black hole at a galactic center (Burrows et al. 2011; Bloom et al. 2011). However, these models may be incompatible with the observed spectra and light curves (see §5.4).

In the collapsar-jet scenario, a longer duration can be simply interpreted by fall-back accretion of a progenitor envelope (Quataert & Kasen 2012; Wu et al. 2013), or direct envelope collapse of a more massive and extended progenitor like blue supergiant (BSG) (e.g., Mészáros & Rees 2001). In this paper, we consider the latter possibility. At first sight, the extended envelope seems problematic for the jet penetration, but the accretion of the massive envelope activates the central engine long enough for the jet to break out the progenitor. Indeed, analytical and numerical calculations showed that relativistic jets from BSG collapsars can penetrate the progenitor envelopes (e.g., Suwa & Ioka 2011; Nagakura et al. 2012) and that the engine activity may last as long as the observed duration of the ULGRBs (e.g., Woosley & Heger 2012).

<sup>1</sup> Department of Physics, Kyoto University, Oiwake-cho, Kitashirakawa, Sakyo-ku, Kyoto 606-8502, Japan

<sup>2</sup> Department of Astronomy & Astrophysics; Department of Physics; Center for Particle & Gravitational Astrophysics; Pennsylvania State University, University Park, PA 16802

<sup>3</sup> Yukawa Institute for Theoretical Physics, Kyoto University, Oiwake-cho, Kitashirakawa, Sakyo-ku, Kyoto 606-8502, Japan

In this paper, we focus on the afterglow phase of ULGRBs. Especially in GRB 111209A afterglow, a J-band bump with AB mag  $\sim 22$  has been confirmed around 10-50 days after the burst (Levan et al. 2013). This emission may reflect the contribution from an underlying SN and is an unique signature of ULGRBs. This underlying SN component is up to  $\lesssim 10$  times brighter than hypernovae associated with LGRBs and is comparable to the so-called superluminous supernovae (SLSNe). We investigate the possibility that such a SLSN-like component is ascribed to a *cocoon-fireball photospheric emission* (CFPE) (Kashiyama et al. 2013). In our previous work, we already proposed the idea that such a CFPE may be a necessary counterpart of BSG GRBs and estimated its basic properties using a simple analytical model. In this paper, we refine our model of the CFPE and explicitly show that the underlying SN component of GRB 111209A afterglow is quite well explained by the CFPE. We also apply our model to the other two bursts, GRB 101225A and GRB 121027A. Then we suggest that some fraction of the observed SLSNe might be originated from the CFPE of off-axis ULGRBs. CFPEs may become a smoking gun of the BSG model for ULGRBs.

This paper is organized as follows. In §2, we review the observational results of ULGRBs. In §3, we propose the BSG model for those ULGRBs. In §4, we explicitly show that the SLSN-like bump of GRB 111209A afterglow can be fitted quite well by the CFPE model. We also apply our model to the other two bursts, GRB 101225A and GRB 121027A. §5 and §6 are devoted to the discussions and summary. In Appendix A, we describe our model and the calculation method in detail.

## 2. ULTRA-LONG GAMMA-RAY BURSTS

In this section, we briefly summarize the observed features of recently detected ULGRBs; GRB 101225A, GRB 111209A, and GRB 121027A. We show some representative features of them in Table 1 (for details, see Gendre et al. 2013; Levan et al. 2013). They all have ultra-long durations of  $\sim 10^4$  s and isotropic energies of  $E_{\gamma, \text{iso}} \sim 10^{52-53}$  erg in prompt phase.<sup>4</sup>

X-ray afterglows were observed by *Swift* X-Ray Telescope (XRT). For GRB 111209A and GRB 121027A, the light curve shapes are similar to those of conventional LGRBs, i.e., consisting of a steep decay, a shallow decay and a normal decay phase (Zhang et al. 2006). The jet breaks have not been confirmed until  $\sim 2 \times 10^6$  s, which gives constraints on the jet opening angles;  $\theta_j > 12^\circ$  (GRB 111209A) and  $\theta_j > 10^\circ$  (GRB 121027A) (Levan et al. 2013). For GRB 101225A, X-ray afterglow is not detected after the end of the steep decay phase  $\sim 10^5$  s and no constraint is given to the jet opening angle (Levan et al. 2013).

A remarkable feature was found in the UV/optical/IR afterglow of GRB 111209A (Levan et al. 2013), which we

<sup>4</sup> Gendre et al. (2013) showed that the estimated spectrum peak energy  $E_p$  and  $E_{\gamma, \text{iso}}$  of GRB 111209A agree with the  $E_p - E_{\gamma, \text{iso}}$  correlation (Amati et al. 2002) within  $2 \sigma$  level. While both prompt emission and X-ray flare of GRB 121027A satisfy the  $E_p - L_p$  correlation (Yonetoku et al. 2004), the  $E_p - E_{\gamma, \text{iso}}$  correlation holds only for the prompt emission (Peng et al. 2013). Physical values of GRB 101225A were not determined well and the relationship with these empirical correlations are uncertain.

mainly discuss in this paper.<sup>5</sup> For  $t_{\text{obs}} \gtrsim 1$  day, the u-band light curve exhibits a single power law decay with  $t^{-1.38}$ , which is similar to X-ray band, while the J-band light curve decays more slowly as  $t^{-0.5}$ . The difference between u-band and J-band temporal indices ( $\sim 0.9$ ) contradicts that predicted from the standard external shock model (0.25) which can be seen from Eq. (A8). Levan et al. (2013) argued that these emissions may be supernova bump, which are clearly different from other GRB-associated SN, and are as bright as the so called superluminous supernovae (SLSNe), which are typically brighter than the normal SN by a factor of  $\sim 100$  (e.g., Gal-Yam 2012). GRB 101225A also showed very shallow temporal decay ( $\propto t^{-0.59}$  in r-band and  $\propto t^{-0.34}$  in i-band) for late-time GRB afterglow. These are also ascribed to an underlying supernova component whose peak luminosity is comparable to the GRB-associated hypernova, SN 1998bw (Levan et al. 2013). Although such a SN-like bump has not been reported yet for GRB 121027A, it may be an unique feature of ULGRBs.

**Table 1**  
Observed Characteristics of ULGRBs.

	111209A	101225A	121027A
$E_{\text{iso}}^{\text{obs}}$ ( $10^{53}$ erg)	$5.8^\dagger$	$\gtrsim 0.12^\ddagger$	$2.0^\diamond$
$\delta t_\gamma^{\text{obs}}$ (s)	$15000^\dagger$	$\gtrsim 2000^\dagger$	$10000^\diamond$
$\theta_j$	$\gtrsim 12^\circ^\ddagger$	—	$\gtrsim 10^\circ^\ddagger$
$z$	$0.677^\dagger$	$0.847^\ddagger$	$1.773^\ddagger$

**Notes.** For GRB 101225A, the prompt emission was already active when *Swift* BAT first slewed to the burst location (Levan et al. 2013), which gives lower limits. GRB 121027A can be divided into the prompt emission with the duration of  $\sim 200$  s, and the giant X-ray flare lasting for  $\sim 10^4$  s (Peng et al. 2013). Here, we include the giant X-ray flare to the prompt phase, given that both of them can be originated from the central engine.

**Reference.**

<sup>†</sup>Gendre et al. (2013), <sup>‡</sup>Levan et al. (2013), <sup>◇</sup>Peng et al. (2013)

## 3. BLUE SUPERGIANT MODEL

In this section, we review the BSG model for ULGRBs. It should be emphasized that this model naturally exhibits the ultra-long duration of these events. In addition, it is predicted that this model accompanies a SLSN-like bright bump in the afterglow phase, which might be actually observed in the optical/infrared band. In this paper, we refer the pre-supernova models to Woosley et al. (2002)<sup>6</sup>, whose data are available from the webpage of Alex Heger<sup>7</sup>. The schematic picture of our model is shown in Fig. 1. We describe details of our model below.

<sup>5</sup> Even before  $t_{\text{obs}} \lesssim 1$  day, some complex features (rebrightening and decay) are seen in the UV/optical/IR light curves. Stratta et al. (2013) performed detailed temporal and spectral analysis of these features. On the contrary, we focus on the afterglow light curves after  $t_{\text{obs}} \gtrsim 1$  day.

<sup>6</sup> In our previous study (Nakauchi et al. 2012), we defined the point where the density becomes  $10^{-7}$  g cm $^{-3}$  as the radius for jet breakout, for stellar models with metallicity of  $10^{-4} Z_\odot$ . Since each stellar model in Woosley et al. (2002) has an outermost density which is different from each other, we adjusted them to the same value. In this paper, following them, we adopted the point of  $10^{-7}$  g cm $^{-3}$  as the effective stellar surface in calculating the jet propagation.

<sup>7</sup> <http://2sn.org/stellarevolution/data.shtml>

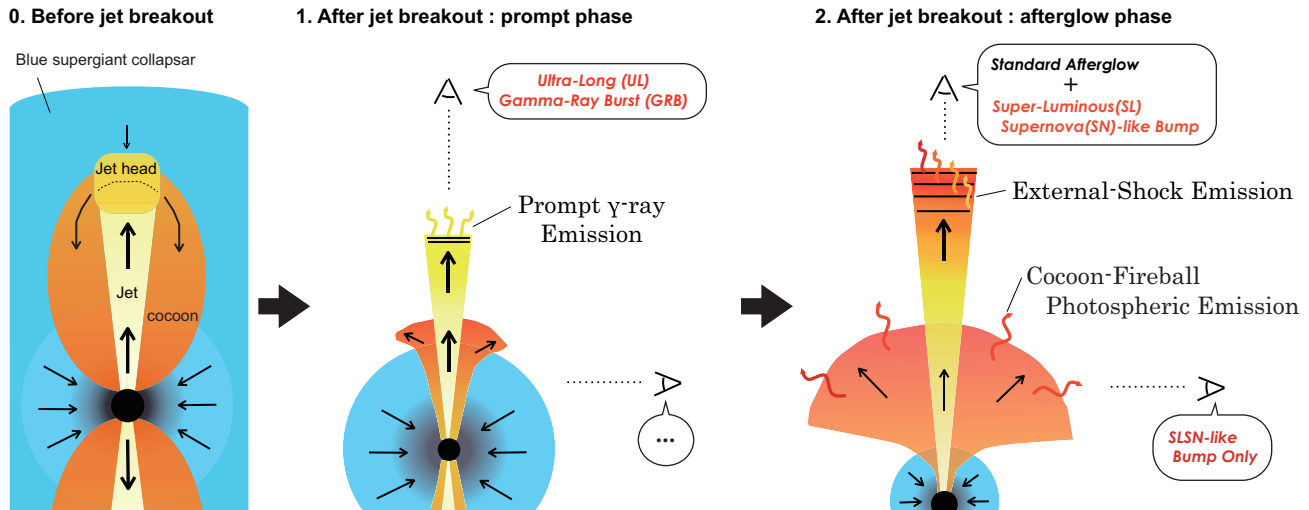


**Figure 1.** The schematic picture of our BSG (blue supergiant) model for ULGRBs (ultra-long gamma-ray burst). 0) Before jet breakout. A jet from the central engine is piercing through a BSG star. The jet head moves with non-relativistic speed forming a hot cocoon. The activity of the central engine continues as far as the envelope matter falls onto the central black hole. 1) After jet breakout: prompt phase. If we observe the event along the jet axis, it is a ULGRB with the duration of  $\sim 10^4$  s. From the off-axis direction, we see nothing or dim orphan emissions. 2) After jet breakout: afterglow phase. Along the jet axis we see the standard afterglow emissions and the CFPE (cocoon-fireball photospheric emission) as a SLSN (superluminous supernova)-like bump. From the off-axis direction, we see only a SLSN-like bump.

Our calculations are based on the collapsar scenario of LGRBs (Woosley 1993; MacFadyen & Woosley 1999). In this scenario, ultra-relativistic jets are launched from the BH accretion disk system which is formed following massive progenitor collapses so that the GRB prompt emission is raised after jets break out the progenitor envelope. The central engine is essentially kept active while the progenitor envelope can be accreted onto it (Kumar et al. 2008) with a typical time scale of

$$\delta t_\gamma \sim t_{\text{ff}}(R_*)(1+z) \sim 77 \left( \frac{R_*}{R_{\text{WR}}} \right)^{3/2} \left( \frac{M_*}{M_{\text{WR}}} \right)^{-1/2} (1+z) \text{ s}, \quad (1)$$

where  $t_{\text{ff}}(r) = \sqrt{r^3/GM_r}$  is the free-fall timescale of a mass shell at mass coordinate  $M_r$  and radius  $r$ . For a WR progenitor with radius  $R_{\text{WR}} \sim 2 \times 10^{10}$  cm and mass  $M_{\text{WR}} \sim 10 M_\odot$  (Woosley et al. 2002), typical durations of observed LGRBs are reproduced from Eq.(1). On the other hand, in order to explain the durations of ULGRBs, one needs to invoke an envelope accretion of a more massive star with an extended progenitor like a blue supergiant (BSG). For example, given a BSG with  $R_* \sim 10^{12}$  cm and  $M_* \sim 50 M_\odot$ , we can estimate the accretion time of the envelope as

$$\delta t_\gamma \sim 1.2 \times 10^4 \left( \frac{R_*}{10^{12} \text{ cm}} \right)^{3/2} \left( \frac{M_*}{50 M_\odot} \right)^{-1/2} (1+z) \text{ s}. \quad (2)$$

Based on this estimate, BSGs were proposed as progenitors of ULGRBs (Gendre et al. 2013; Kashiyama et al. 2013). According to the stellar evolution theory, metal poor stars end as BSGs with massive hydrogen envelopes

and typical radii of  $10^{12} - 10^{13}$  cm. This is because the low opacity envelope suppresses the line-driven mass loss from the stellar surface (Woosley et al. 2002). Metal poor stars with mass of  $40 - 140 M_\odot$  are considered to form black holes with little mass ejection (Heger et al. 2003). Thus, by considering a metal-poor BSG like collapsar, we can expect that the very long duration of ULGRBs are natural outcomes (e.g., Woosley & Heger 2012).

Some LGRB afterglow light curves show bumps in UV/optical/IR band, which imply the presence of underlying SNe (Woosley & Bloom 2006). So far, nearly a dozen of LGRBs are confirmed to accompany type Ic supernovae, which implies WR stars as progenitors. Thus UV/optical/IR afterglow provides us a key to determine the progenitor of GRBs. As we saw in the previous section, GRB 111209A afterglow shows a J-band bump and the accompanying SLSN-like component is suggested. This association, however, seems problematic for the BSG model, because SN explosions may fail for massive BSGs. If BSGs succeeded in SN explosions in some way, this time, a large fraction of the progenitor envelope would be ejected away to suppress the long lasting accretion onto the central engine. This dilemma forced us to consider another mechanism of SLSN-like bump, which is CFPE (cocoon-fireball photospheric emission).

In this paper, by considering jet-cocoon structure in the collapsar envelope, we interpret the SLSN-like bump as the CFPE, which strengthens our previous proposal that the progenitor of a ULGRB is a BSG-like star (Kashiyama et al. 2013). While a collapsar jet is piercing through the progenitor envelope, jet energy is dissipated at the jet head and is stored in a cocoon consist-

ing of hot plasma (Matzner 2003). Along with the jet breakout, cocoon also breaks out the progenitor and its dynamics can be regarded as a non-relativistic fireball. Kashiyama et al. (2013) modeled the photospheric emission from an expanding cocoon fireball in a rather simple manner. We here refine our model so as to explain the observed features. To make the paper easier to read for non-experts, we show the details of numerical methods in the Appendix.

#### 4. COCOON-FIREBALL PHOTOSPHERIC EMISSION AS A SUPERLUMINOUS-SUPERNOVA-LIKE BUMP OF ULTRA-LONG GAMMA-RAY BURST

In this section, we first focus on the SLSN-like bump of GRB 111209A. Based on the BSG model, we show that such a bright UV/optical/IR emission can be interpreted as the cocoon-fireball photospheric emission (CFPE). Then, we apply our model to other two events, and discuss the possible constraints.

The calculation methods we use are shown in Appendix in detail. The schematic picture of our model is shown in Fig. 1. Below, we overview our methods;

- First, we give the progenitor model, and the jet opening angle  $\theta_j$ . Then, for a fixed jet efficiency  $\eta_j$ , we calculate the jet propagation within the progenitor envelope, and determine the jet breakout time  $t_{\text{bo}}$  based on our previous works (Suwa & Ioka 2011; Nakauchi et al. 2012; Kashiyama et al. 2013). By calculating the mass accretion rate after breakout, we determine the duration of the prompt emission  $\delta t_\gamma$ .  $\eta_j$  is adjusted so as to reproduce the observed duration  $\delta t_\gamma^{\text{obs}}$ . Cocoon parameters at breakout,  $E_c(t_{\text{bo}})$  and  $M_c(t_{\text{bo}})$  are obtained at this stage (see §A.1 and §A.2).
- Second, by considering the jet luminosity after breakout, we determine the isotropic energy  $E_{\text{iso}}$  in prompt phase. A constant radiation efficiency  $\epsilon_\gamma$  is introduced and is adjusted so as to reproduce the observed  $E_{\text{iso}}^{\text{obs}}$ . Thus,  $\eta_j$  and  $\epsilon_\gamma$  are chosen appropriately for a given  $\theta_j$  and progenitor model. The kinetic energy of the relativistic ejecta  $E_{\text{kin}}$  is obtained at this stage (see §A.2).
- Third, we calculate the afterglow emissions following the standard external shock model in Sari et al. (1998), and compare our results with the observed X-ray light curves (LCs). To begin with, from the X-ray LC slope, the power law index of the accelerated electron's energy spectrum  $p$  is determined. Then, the electron acceleration efficiency  $\epsilon_e$  is strongly constrained from the observed X-ray flux, due to the large dependence of the theoretical flux on  $\epsilon_e$ , i.e.,  $F_{(0.3-10 \text{ keV})} \propto \epsilon_e^{3/2} \epsilon_B^{1/8} n^0$  (see §A.3 and Eq. A8 with  $p = 2.5$ ).
- Fourth, we calculate the CFPEs, using  $E_c(t_{\text{bo}})$  and  $M_c(t_{\text{bo}})$  as the initial parameters of the cocoon fireball. We suppose that the CFPE contributes dominantly to the optical/IR bump. CFPE is attenuated by the host galaxy, and the V-band extinction in host galaxy,  $A_V^{\text{host}}$ , is adjusted so as to reproduce

the observed SN-like bump in optical/IR band (see §A.4).

- Finally, we suppose that the UV flux is dominantly contributed from the external shock emission. For typical parameters, UV flux can be calculated from  $F_{\text{UV}} \propto \epsilon_e^{3/2} \epsilon_B^{7/8} n^{1/2}$  (see Eq. A8 with  $p = 2.5$ ). From the observed UV flux, the appropriate value of the magnetic field amplification efficiency  $\epsilon_B$  is obtained for a given ambient gas density  $n$ . Thus, if we give the ambient gas density  $n$ , afterglow parameters,  $\epsilon_e$ ,  $\epsilon_B$ , and  $p$  are set appropriately from the X-ray and UV observations (see §A.3).

In summary, we have 6 constraints from the observations against 8 unknown parameters. As the two free parameters, we choose  $\theta_j$  and the ambient gas density  $n$ . In this study, as for the progenitor, we adopt the BSG model with zero age main sequence (ZAMS) mass of  $75 M_\odot$  and metallicity of  $10^{-4} Z_\odot$  calculated by Woosley et al. (2002).<sup>8</sup> In the pre-collapse phase, this BSG has mass  $M_* \sim 75 M_\odot$  and radius  $R_* \sim 8.6 \times 10^{12}$  cm. If we give the jet opening angle  $\theta_j$  and the ambient gas density  $n$ , we can calculate all the features of ULGRBs both in prompt and afterglow phases. The model parameters, which fit the observational data, are summarized in Table 2.

**Table 2**

Model parameters and calculated quantities with zero age main sequence (ZAMS) mass of  $75 M_\odot$  and metallicity of  $10^{-4} Z_\odot$  calculated by Woosley et al. (2002)

	111209A	101225A	121027A
$\theta_j$	$12^\circ$	$12^\circ$	$12^\circ$
$\eta_j$	$1.24 \times 10^{-3}$	$6.2 \times 10^{-4}$	$1.24 \times 10^{-3}$
$\epsilon_\gamma$	0.38	0.7	0.1
$p$	2.5	2.1	2.6
$\epsilon_e$	0.01	$5 \times 10^{-4}$	0.05
$\epsilon_B$	$1 \times 10^{-3}$	0.05	$8 \times 10^{-4}$
$n$ ( $\text{cm}^{-3}$ )	0.04	0.1	0.01
$A_V^{\text{host}}$ (mag)	0.26	0.58	1.1
$E_{\text{iso}}$ ( $10^{53}$ erg)	5.9	2.4	1.5
$\delta t_\gamma$ (s)	9000	5100	15000
$E_{\text{kin}}$ ( $10^{53}$ erg)	9.6	1.0	14
$E_c(t_{\text{bo}})$ ( $10^{53}$ erg)	1.0	0.56	1.0
$M_c(t_{\text{bo}})$ ( $M_\odot$ )	5.8	7.0	5.8

#### 4.1. GRB 111209A

For GRB 111209A, we set the jet opening angle as  $\theta_j = 12^\circ$ , which is the lower limit given by the non-detection of the jet break in the X-ray afterglow (Levan et al. 2013). In this case, the observed isotropic energy  $E_{\text{iso}}^{\text{obs}} \sim 5.8 \times 10^{53}$  erg and the duration  $\delta t_\gamma^{\text{obs}} \sim 15000$  s (Gendre et al.

<sup>8</sup> The observations suggested that the ULGRB host galaxies have sub-solar metallicities, and that as long as we consider BSG progenitors, they might be originated from massive star binary systems rather than single low metal massive stars (Stratta et al. 2013). However the stellar structure is not so different in BSGs, so that our progenitor can be regarded as a representative model applicable for any scenario, i.e., either the consequence of single star evolution or binary evolution.

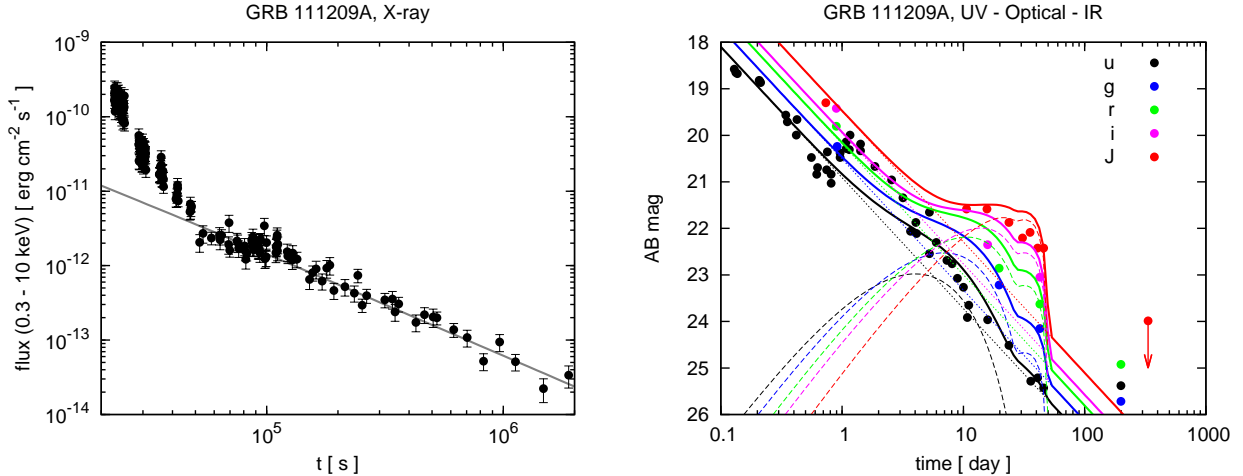


**Figure 2.** Theoretical fitting of GRB 111209A afterglow light curves (LCs). The left panel shows the LC in XRT range and the right one is in UV/optical/IR range, where the points represent the observed data, and the solid lines correspond to the theoretical model in X (grey), u (black), g (blue), r (green), i (magenta) and J (red) bands, respectively. While the observations are shown as filled circles with the same colors, respectively. We use a BSG progenitor with zero age main sequence (ZAMS) mass of  $75 M_{\odot}$  and  $10^{-4} Z_{\odot}$ . We find that if we give  $\theta_j = 12^{\circ}$  and  $n = 0.04 \text{ cm}^{-3}$ , other parameters are determined from the observations as  $\eta_j = 1.24 \times 10^{-3}$ ,  $\epsilon_{\gamma} = 0.38$ ,  $p = 2.5$ ,  $\epsilon_e = 0.01$ ,  $\epsilon_B = 1 \times 10^{-3}$ , and  $A_V^{\text{host}} = 0.26$  (see Table 2). In the right panel, the thin-dotted lines correspond to the external shock components. The SLSN-like bump, which dominates at later phase, is well reproduced by the CFPE (thin-dashed lines) with  $E_c(t_{\text{bo}}) = 1.0 \times 10^{53}$  erg and  $M_c(t_{\text{bo}}) = 5.8 M_{\odot}$ . We see that the theoretical curves reproduce the observations quite well. In the right panel, the error bars are smaller than the data points in *J*, *i*, *r*, and *g*-bands. But in *u*-band, some error bars are larger than the point size, and are  $\pm 0.5$  mag at most. The data points at  $\sim 200$  day may reflect the emissions from the host galaxy (see Levan et al. 2013, for details).

2013) are substantially reproduced by setting the jet efficiency and the radiation efficiency as  $\eta_j = 1.24 \times 10^{-3}$  and  $\epsilon_{\gamma} = 0.38$ , respectively. The above set of parameters ( $\theta_j, \eta_j, \epsilon_{\gamma}$ ) determines the kinetic energy of the relativistic ejecta as  $E_{\text{kin}} = 9.6 \times 10^{53}$  erg, and the internal energy and the baryon mass of the cocoon as  $E_c(t_{\text{bo}}) = 1.0 \times 10^{53}$  erg and  $M_c(t_{\text{bo}}) = 5.8 M_{\odot}$ , respectively (see Table 2).

The left panel of Fig. 2 shows the XRT afterglow LC (black dots with error bars) and the theoretical fitting (solid gray line). The right panel of this figure shows the UV/optical/IR afterglow LCs and the theoretical fittings for u (black), g (blue), r (green), i (magenta), and J (red) bands. The data points at  $\sim 200$  day may reflect the host galaxy contribution (Levan et al. 2013). We focus on the normal decay phase starting at  $t_{\text{obs}} \sim 10^5$  s. The observed X-ray flux decays as  $t^{-1.36}$  for  $t \gtrsim 10^5$  s (Levan et al. 2013). This gives the power law index of non-thermal electrons as  $p = 2.5$ . The X-ray and u-band fluxes are reproduced by setting the ambient gas density, the electron acceleration efficiency, and the magnetic field amplification efficiency as  $n = 0.04 \text{ cm}^{-3}$ ,  $\epsilon_e = 0.01$  and  $\epsilon_B = 1 \times 10^{-3}$ , respectively. One can see that the standard-afterglow components (thin-dotted lines) roughly illustrate the observed data for 1 day  $\lesssim t_{\text{obs}} \lesssim 5$  day,<sup>9</sup> and the SLSN-like bump dominates in optical/IR bands for  $t_{\text{obs}} \gtrsim 5$  day. We find that by setting  $A_V^{\text{host}} = 0.26$  mag, the CFPEs (thin-

<sup>9</sup> One can see that there is a re-brightening in u-band at  $\sim 1$  day, which also cannot be explained by the standard external shock model. Our target here is, however, the SLSN-like component emerged after  $\sim 10$  day. So, for simplicity, we treat the power law component of the afterglow within the standard model. Detailed theoretical interpretations of this re-brightening are discussed in Stratta et al. (2013).

dashed lines) explain the SLSN-like bump quite well.

The model parameters for the above fittings have reasonable values (see Table 2). Thus, we can conclude that ULGRB 111209A and the accompanying SLSN-like bump are well reproduced by the BSG collapsar model. Note that since the CFPEs are calculated based on a TypeIIP SN model, the observed bump may be able to be explained by a SN ejecta, not by a cocoon. However, a significantly large explosion energy of  $\sim 10^{53}$  erg ( $\sim$  a third of the binding energy of the neutron star) is still necessary, which would be very difficult as far as we consider standard spherical explosions.

#### 4.2. GRB 101225A

For GRB 101225A, it is relatively hard to constrain our model parameters, since we only have a lower limit to the duration and the isotropic energy of the prompt emission, and no constraint is given to the opening angle. Here, we assume the same opening angle  $\theta_j = 12^{\circ}$  as GRB 111209A, and take fiducial values for the jet efficiency,  $\eta_j = 6.2 \times 10^{-4}$  and the radiation efficiency,  $\epsilon_{\gamma} = 0.7$ . The parameter set gives  $\delta t_{\gamma} \sim 5100$  s and  $E_{\text{iso}} = 2.4 \times 10^{53}$  erg, which exceed the observed lower limits, and  $E_{\text{kin}} = 1.0 \times 10^{53}$  erg is also obtained. Cocoon parameters are also calculated as  $E_c(t_{\text{bo}}) = 5.6 \times 10^{52}$  erg and  $M_c(t_{\text{bo}}) = 7.0 M_{\odot}$ , respectively.

The left panel of Fig. 3 shows the afterglow LC in XRT band. For  $t_{\text{obs}} > 10^5$  s, only an upper limit is given, and the normal decay phase is not confirmed. Thus, the afterglow parameters are also hardly constrained from the observation. We find that the theoretical LC (grey solid line) is basically consistent with the observed upper limit for  $\epsilon_e < 5 \times 10^{-4}$ . The right panel of Fig. 3 shows the afterglow LCs in i (magenta) and r (green) bands. Here we divide the LCs into two phases by  $t_{\text{obs}} \sim 5$  day.

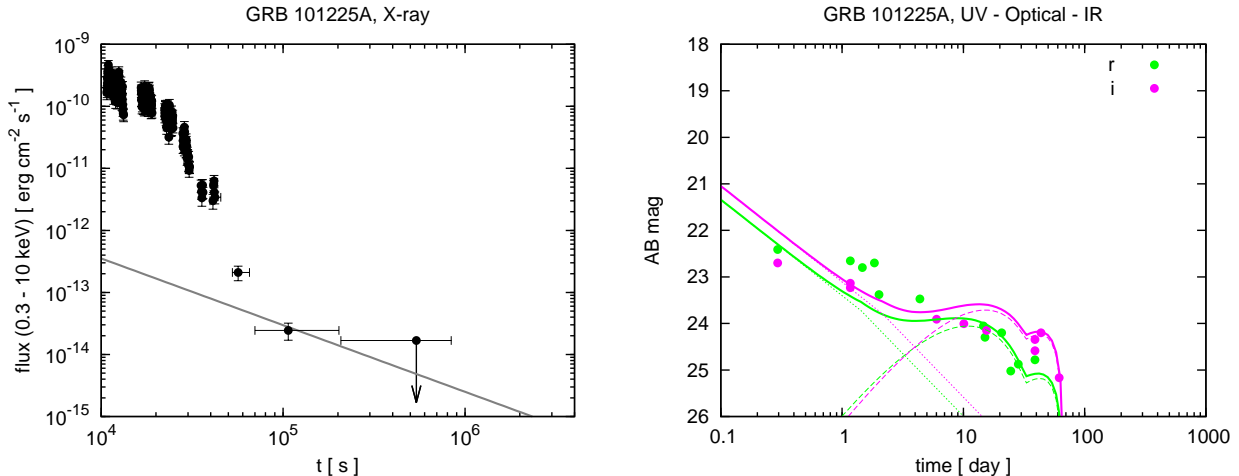


**Figure 3.** Same as Fig. 2, but for GRB 101225A. Despite large uncertainties, the observed features are consistent with the BSG model, where the external shock components dominate at earlier phase (thin-dotted lines) and the CFPE dominates at later phase (thin-dashed lines) with  $E_c(t_{\text{bo}}) = 5.6 \times 10^{52}$  erg and  $M_c(t_{\text{bo}}) = 7.0 M_\odot$ . Here, the progenitor model is the same as Fig. 2. We have only two observational constraints in r (green) and i (magenta) bands. Nevertheless for a given set of parameters such as  $\theta_j = 12^\circ$ ,  $\eta_j = 6.2 \times 10^{-4}$ ,  $\epsilon_\gamma = 0.7$ ,  $p = 2.1$ ,  $\epsilon_e = 5 \times 10^{-4}$ , and  $n = 0.1 \text{ cm}^{-3}$ , the remaining parameters are determined from the observations as  $\epsilon_B = 0.05$  and  $A_V^{\text{host}} = 0.58$  (see Table 2). The theoretical curves reproduce the observations rather well. In the right panel, the error bars are less than  $\pm 0.25$  mag in each band (see Levan et al. 2013, for details).

In the earlier phase, we suppose that the standard afterglow emissions (thin-dotted lines) dominate, and find that the observed LCs are fitted with a given set of the parameters,  $p = 2.1$ ,  $n = 0.1 \text{ cm}^{-3}$ ,  $\epsilon_e = 5 \times 10^{-4}$ , and  $\epsilon_B = 0.05$ . In the later phase, the HN-like bump dominates (Levan et al. 2013), and it can be fitted by the CFPEs (thin-dashed lines) with  $A_V^{\text{host}} = 0.58$ .

Although the uncertainties are relatively high, one can see that the prompt and afterglow emissions of GRB 101225A are consistent with the BSG model.

#### 4.3. GRB 121027A

GRB 121027A consists of the prompt phase for  $t_{\text{obs}} < 200$  s and the giant X-ray flare phase for  $200 \text{ s} < t_{\text{obs}} < 10^4$  s. In this paper, we suppose that this giant X-ray flare is also related to the central engine activity, and both phases are due to the activity of the jets. We set the jet opening angle as  $\theta_j = 12^\circ$ , which is consistent with a constraint of  $\theta_j > 10^\circ$  (Levan et al. 2013). By adopting  $\eta_j = 1.24 \times 10^{-3}$  and  $\epsilon_\gamma = 0.1$ , the observed prompt emission is roughly reproduced as  $E_{\text{iso}} = 1.5 \times 10^{53}$  erg and  $\delta t_\gamma \sim 15000$  s<sup>10</sup>. The kinetic energy of the relativistic ejecta and the cocoon parameters are given as  $E_{\text{kin}} = 1.4 \times 10^{54}$  erg,  $E_c(t_{\text{bo}}) = 1.0 \times 10^{53}$  erg, and  $M_c(t_{\text{bo}}) = 5.8 M_\odot$ , respectively (see Table 2).

In Fig. 4, we show the afterglow LCs in XRT (left panel) and UV/optical/IR band (right panel). In the right panel, each color corresponds to g' (blue), r' (green), i' (magenta), and J (red) band, respectively. We find that the XRT LC for  $t_{\text{obs}} \gtrsim 2 \times 10^5$  s can be fitted well with  $p = 2.6$  and  $\epsilon_e \approx 0.05$ . For UV/optical/IR band, the observed data have been reported only at

$t_{\text{obs}} \sim 2.05$  day (Kruehler et al. 2012). Provided that the observed fluxes at  $t_{\text{obs}} \sim 2.05$  day are attributed to the standard afterglow emissions, they are reproduced by setting  $n = 0.01 \text{ cm}^{-3}$ ,  $\epsilon_B = 8 \times 10^{-4}$ , and  $A_V^{\text{host}} = 1.1$  (right panel). The CFPEs are shown with thin-dashed lines, which slightly exceed the standard afterglow components in optical/IR bands at  $t_{\text{obs}} \sim 20$ -80 day. For this burst, the standard afterglow components are relatively bright due to the high acceleration efficiency of relativistic electrons,  $\epsilon_e$  (see Table 2). So the CFPEs are almost buried compared to the standard afterglow components, although CFPEs are as bright as the observed SLSNe. We predict that a SLSN-like bump might have appeared at  $t_{\text{obs}} \sim 20$ -80 day in the optical/IR afterglow light curve of GRB 121027A.

## 5. DISCUSSIONS

### 5.1. Possible Subclass of SLSNe from Off-axis ULGRBs?

In the previous section, we show that a ULGRB with a SLSN-like bump, in particular GRB 111209A, can be interpreted by the collapsar-jet scenario of BSG progenitors. The prompt gamma-ray emissions and the standard afterglow emissions are attributed to a relativistic jet, while the SLSN-like bump comes from a non-relativistic cocoon fireball. In this model, only the SLSN-like component may be seen, if the observer locates along the off-axis direction from the ULGRB jet, due to the relativistic beaming effect. Then we can propose that a fraction of SLSNe are originated from off-axis ULGRBs. Indeed, the anticipated event rate of such off-axis ULGRBs can be not much less than that of the observed SLSNe (Kashiyama et al. 2013). This conjecture can be tested, for example, by searching the orphan afterglow of a ULGRB associated with a SLSN. After the relativistic jet is decelerated enough, it begins to spread sideways to become a mildly-relativistic spherical ejecta and after-

<sup>10</sup> While we use the same values for  $\theta_j$  and  $\eta_j$  with those for GRB 111209A, the calculated duration  $\delta t_\gamma \sim 15000$  s is larger than that of GRB 111209A ( $\delta t_\gamma \sim 9000$  s) calculated in §4.1. This is because GRB 121027A has higher redshift of  $z = 1.773$  than that of GRB 111209A ( $z = 0.677$ ).

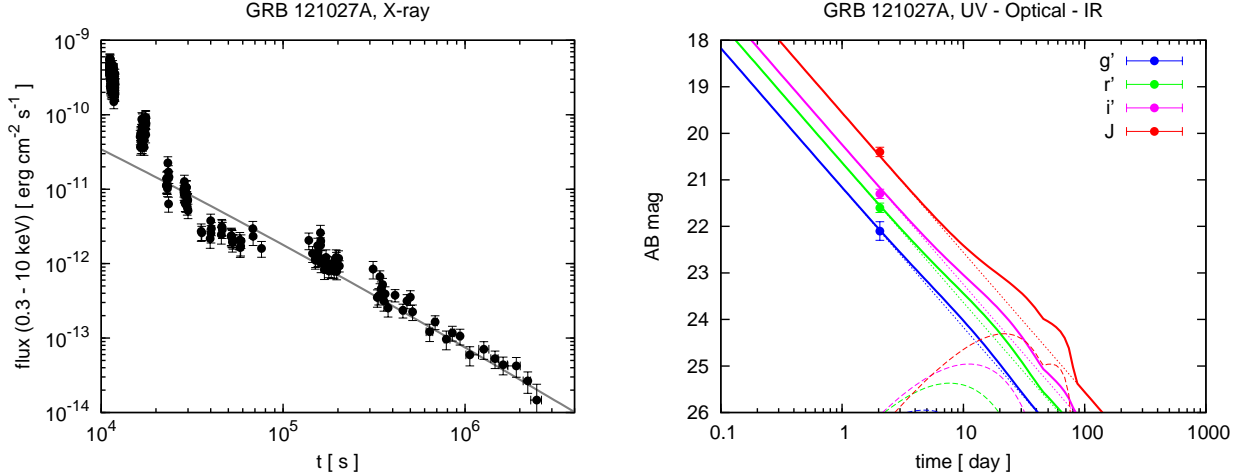


**Figure 4.** Same as Fig. 2, but for GRB 121027A. We find that the observed features are consistent with the BSG model, where we adopt the same progenitor model with Fig. 2. Since the observational data of the SN component are not available in this case, we need to fix three parameters. If we give  $\theta_j = 12^\circ$ ,  $n = 0.01 \text{ cm}^{-3}$ , and  $A_V^{\text{host}} = 1.1$ , for example, other parameters are determined from the observations as  $\eta_j = 1.24 \times 10^{-3}$ ,  $\epsilon_\gamma = 0.1$ ,  $p = 2.6$ ,  $\epsilon_e = 0.05$ , and  $\epsilon_B = 8 \times 10^{-4}$  (see Table 2). In the right panel, we suppose that the observed data at  $\sim 2.05$  day reflect the external shock emissions (thin-dotted lines). The cocoon parameters are calculated as  $E_c(t_{\text{bo}}) = 1.0 \times 10^{53}$  erg and  $M_c(t_{\text{bo}}) = 5.8 M_\odot$ . We can predict that a SLSN-like bump derived from the CFPE (thin-dashed lines) might have been observed for  $\sim 20$ -80 days after the burst.

glow emissions can be seen as an orphan afterglow for off-axis observers afterward it (e.g., Rhoads 1997; Sari et al. 1999). Thus, the simultaneous and the follow-up observations in optical or radio bands would play a key role for testing the proposed association. Note that, by stacking the proposed SLSNe, we might also detect GeV-TeV neutrinos, which are produced during the jet propagation inside BSG progenitors (Murase & Ioka 2013).

## 5.2. Parameter and Progenitor Dependence

Here, we present the parameter dependence of our model. First, let us discuss the jet propagation inside a progenitor. For a fixed jet efficiency  $\eta_j$ , a broader jet opening angle  $\theta_j$  gives a slower jet head. If the jet head cannot reach the surface of the progenitor before the engine stops, i.e.,  $\dot{M}(t) \lesssim 10^{-3} M_\odot \text{ s}^{-1}$  (see Appendix A.1), the jet fails to penetrate the progenitor. In particular, we find that for a fiducial jet efficiency  $\eta_j = 6.2 \times 10^{-4}$ , jets fail to penetrate the progenitor BSG for  $\theta_j \gtrsim 18^\circ$ . For twice energetic jets with  $\eta_j = 1.24 \times 10^{-3}$ , they fail to penetrate for  $\theta_j \gtrsim 24^\circ$ . On the other hand, for a fixed  $\theta_j$ , there is a lower limit of  $\eta_j$  for the jet penetration. For the BSG progenitor with  $\theta_j = 12^\circ$ , jets are possible to penetrate the envelope for  $\eta_j \gtrsim 3.1 \times 10^{-4}$ .

CFPEs are also affected by  $\theta_j$  and  $\eta_j$ . The duration and the luminosity of CFPEs roughly scale with the internal energy  $E$ , the baryon mass  $M$ , and the initial cocoon-fireball radius  $R_0$  as

$$\delta t_{\text{CFPE}} \propto M^{3/4} E^{-1/4}, \quad (3)$$

$$L_{\text{CFPE}} \propto M^{-1} E R_0. \quad (4)$$

Eqs. (3) and (4) can be easily derived if we remind the fact that  $\delta t_{\text{CFPE}}$  is determined by the equality between the photon diffusion time and the dynamical time  $R(t)/v_{\text{sc}}$  of the CFPE, while the luminosity is derived from the photon diffusion equation at  $\delta t_{\text{CFPE}}$ . We find

that for a fixed  $\eta_j$ ,  $M$  increases with  $\theta_j$ , while  $E$  hardly changes. Therefore, one can expect a longer and dimmer CFPE for a larger  $\theta_j$ . On the other hand, for a fixed  $\theta_j$ ,  $E$  increases with  $\eta_j$ , while  $M$  hardly changes. Therefore, one can expect a shorter and brighter CFPE for a larger  $\eta_j$ .

We also study the progenitor dependence of our model. For that purpose, we fix the central engine parameters as  $\theta_j = 12^\circ$  and  $\eta_j = 1.24 \times 10^{-3}$ , which are the same as those used in §4.1 and are applied to the massive ( $75 M_\odot$ ) BSG progenitor. We confirm that a lower mass BSG progenitor can reproduce the observed features of UL-GRB prompt emissions. For example, if we consider a BSG with pre-collapse mass  $M_* = 40 M_\odot$  and radius  $R_* = 4.4 \times 10^{12}$  cm (Woosley et al. 2002), the duration and the isotropic energy of GRB 111209A are roughly reproduced as  $\delta t_\gamma \sim 6500$  s and  $E_{\gamma, \text{iso}} = 5.5 \times 10^{53}$  erg, respectively, with  $\theta_j = 12^\circ$ ,  $\eta_j = 1.24 \times 10^{-3}$ , and  $\epsilon_\gamma = 0.5$ . Cocoon parameters are also calculated as  $E_c(t_{\text{bo}}) = 5.6 \times 10^{52}$  erg and  $M_c(t_{\text{bo}}) = 7.0 M_\odot$ . In this case, the CFPEs at  $z = 0.677$  have the peak magnitude of  $\sim 23$  mag (with extinction of  $A_V^{\text{host}} = 0.26$  mag) in J-band and the duration of  $\sim 10$ -30 day. Note that for the massive BSG progenitor case, the peak magnitude of the CFPE is  $\sim 22$  mag (with extinction of  $A_V^{\text{host}} = 0.26$  mag) in J-band and the emission timescale is  $\sim 20$ -40 day (see Fig. 2). We find that while the duration of the CFPEs slightly differs, the luminosity of the CFPEs from the lower mass BSG becomes several times lower than those from the more massive BSG progenitor. Thus, we can infer the mass or radius of a BSG progenitor from the observation of CFPEs (see also Kashiyama et al. 2013).

We also find that WR progenitors cannot explain the observed SLSN-like bump in light of both the luminosity and the duration. A WR progenitor with ZAMS mass  $40 M_\odot$  and metallicity  $Z_\odot$  has mass  $M_* = 8.7 M_\odot$  and radius  $R_* = 2.3 \times 10^{10}$  cm in the pre-collapse phase

(Woosley et al. 2002). We calculate the CFPEs from this WR progenitor by applying our model with  $\theta_j = 12^\circ$  and  $\eta_j = 1.24 \times 10^{-3}$ , which give the cocoon parameters as  $E_c(t_{\text{bo}}) = 7.3 \times 10^{51}$  erg and  $M_c(t_{\text{bo}}) = 0.33 M_\odot$ , respectively. We find that the peak magnitude of the CFPEs at  $z = 0.677$  becomes  $\sim 27$  mag (with extinction of  $A_V^{\text{host}} = 0.26$  mag) in J-band, which is almost 100 times dimmer than those for the massive ( $75 M_\odot$ ) BSG progenitor case. The light curve peak is reached on  $\sim 3$  day in J-band, which is much earlier than that of the BSG progenitor case. From these results, we conclude that bright CFPEs may be an unique characteristic of GRBs from BSG progenitors (see also Kashiyama et al. 2013).

### 5.3. CFPEs from Population III GRBs

An interesting application of the BSG model is to Population III (Pop III) stars, metal-free stars formed dominantly at high redshifts. Pop III stars are considered to become massive BSGs in their pre-collapse phase because of their metal-free envelopes, although the typical mass has a large theoretical uncertainty, i.e.,  $\sim 10 - 10^3 M_\odot$  (e.g., Abel et al. 2002; Bromm et al. 2002; Tan & McKee 2004; McKee & Tan 2008; Hosokawa et al. 2011). This implies that Pop III GRBs can be seen as ULGRBs, and they potentially dominate at higher redshifts if the BSG model holds. For broad mass range of Pop III BSG progenitors, many authors have argued that both prompt and standard afterglow signals of Pop III GRBs would be detectable using future facilities (Mészáros & Rees 2010; Komissarov & Barkov 2010; Suwa & Ioka 2011; Nagakura et al. 2012; Nakauchi et al. 2012; Kashiyama et al. 2013).

As we have discussed so far, bright CFPEs may be common characteristics of BSG GRBs. In addition to the prompt and standard afterglow emissions, CFPEs from Pop III GRBs will be detectable even at  $z \gtrsim 10$  with future facilities like *JWST* NIRCcam (Kashiyama et al. 2013), which will provide us valuable information about the star formation history in the high- $z$  universe.

### 5.4. Other Scenarios of ULGRBs

Finally, we here discuss other possible scenarios proposed to explain ULGRBs.

For GRB 101225A, two different scenarios were proposed just after the discovery. One is the tidal disruption of a minor body by a galactic neutron star (Campana et al. 2011), and the other is related to the stellar merger of a neutron star with a helium star at  $z = 0.33$  (Thöne et al. 2011). Now we know that the observed ULGRBs are extragalactic origin, the former galactic scenario is unlikely. On the other hand, the latter scenario predicts that afterglow emissions are suppressed as in GRB 101225A, and thus cannot be directly applied to GRB 111209A and 121027A.

In collapsar-jet scenario, a longer activity of a central engine can be realized by implementing a fall-back accretion (Quataert & Kasen 2012). In fact, Wu et al. (2013) divide GRB 121027A into a prompt phase with a duration of  $\sim 200$  s and an X-ray-flare phase with  $\sim 10^4$  s, and showed that the X-ray flare with a sharp rising can be explained by a fall-back accretion of falling back mass  $M_{\text{fb}} \sim 0.9 - 2.6 M_\odot$  from the radius  $r_{\text{fb}} \sim 3.5 \times 10^{10}$  cm. Although our model does not take into account the effect

of fall-back accretion, the BSG model itself is compatible with this interpretation, since the fall-back accretion can naturally occur in massive BSGs.

Shock-breakout scenario can also reproduce the observed duration of ULGRBs by implementing a large breakout radius,  $c \delta t_\gamma \sim 3 \times 10^{14} (\delta t_\gamma / 10^4 \text{ s}) \text{ cm}$  (Colgate 1974; Klein & Chevalier 1978; Ensman & Burrows 1992; Matzner & McKee 1999). However, shock-breakout emissions would show relatively smooth light curves and quasi-thermal spectra (e.g., Waxman et al. 2007; Nakar & Sari 2012), which is not the case for the observed ULGRBs.

Tidal disruptions of stars by supermassive black holes can also give long lasting emissions (Burrows et al. 2011; Bloom et al. 2011). However, the observed tidal disruption events have isotropic luminosities  $\lesssim 10^{48} \text{ erg s}^{-1}$ , which are orders-of-magnitude dimmer than ULGRBs ( $\gtrsim 10^{49} \text{ erg s}^{-1}$ ). Also, this scenario predicts a prompt light curve with temporal dependence  $\propto t^{-5/3}$  (Rees 1988; Phinney 1989), which is inconsistent with the observed ULGRBs.

## 6. SUMMARY

ULGRBs have durations of  $\sim 10^4$  s, which is much longer than that of LGRBs ( $\sim 30$  s). The observed afterglow light curves show SLSN-like bumps, which are  $\lesssim 10$  times brighter than a GRB-associated hypernova, SN 1998bw. Such long durations are naturally explained, if we consider BSG collapsars rather than WR collapsars, since the accretion of a massive hydrogen envelope activates the central engine for a long duration. In the BSG model, ULGRBs necessarily accompany SLSN-like transients in afterglow phase, as shown in Kashiyama et al. (2013). They considered photospheric emissions from the expanding cocoon fireball, which is formed during the jet propagation in the progenitor and breaks out the progenitor along with the jet. In this paper, we refine our previous model for cocoon-fireball photospheric emissions (CFPEs), and interpret the observed SLSN-like bump as the CFPE. For GRB 111209A and GRB 101225A, we find that if we have enough observations, i.e., the duration, isotropic energy, X-ray and UV/optical/IR afterglow light curves, and SLSN-like bump, the observed features of a ULGRB and SLSN-like bump are reproduced quite well, for a given set of the progenitor model; the jet opening angle, and the ambient gas density. For GRB 121027A, UV/optical/IR afterglow data after  $t_{\text{obs}} = 2.05$  day are not published yet, and we predict that SLSN-like bump might have been observed for  $\sim 20$ -80 days after the burst.

## ACKNOWLEDGEMENTS

We thank K. Ioka, T. Enoto, and T. Sakamoto for fruitful discussions and comments. We also thank P. Mészáros, B.B. Zhang, P. Veres, and K. Murase for valuable discussions. This work is supported in part by the Grant-in-Aid from the Ministry of Education, Culture, Sports, Science and Technology (MEXT) of Japan, Nos. 23540305 (TN), 24103006 (TN), 23840023 (YS), 25103511 (YS), JSPS Postdoctoral Fellowship for Research Abroad (KK), and NASA NNX13AH50G (KK).

## REFERENCES



- Abel, T., Bryan, G. L., & Norman, M. L. 2002, *Science*, 295, 93
- Amati, L., Frontera, F., Tavani, M., et al. 2002, *A&A*, 390, 81
- Arnett, W. D. 1980, *ApJ*, 237, 541
- Bloom, J. S., Giannios, D., Metzger, B. D., et al. 2011, *Science*, 333, 203
- Bromm, V., Coppi, P. S., & Larson, R. B. 2002, *ApJ*, 564, 23
- Burrows, D. N., Kennea, J. A., Ghisellini, G., et al. 2011, *Nature*, 476, 421
- Campana, S., Mangano, V., Blustin, A. J., et al. 2006, *Nature*, 442, 1008
- Campana, S., Lodato, G., D’Avanzo, P., et al. 2011, *Nature*, 480, 69
- Chen, W.-X., & Beloborodov, A. M. 2007, *ApJ*, 657, 383
- Colgate, S. A. 1974, *ApJ*, 187, 333
- Covino, S., Melandri, A., Salvaterra, R., et al. 2013, arXiv:1303.4743
- Ensmann, L., & Burrows, A. 1992, *ApJ*, 393, 742
- Gal-Yam, A. 2012, *Science*, 337, 927
- Gendre, B., Stratta, G., Atteia, J. L., et al. 2013, *ApJ*, 766, 30
- Ghirlanda, G., Ghisellini, G., & Lazzati, D. 2004, *ApJ*, 616, 331
- Heger, A., Fryer, C. L., Woosley, S. E., Langer, N., & Hartmann, D. H. 2003, *ApJ*, 591, 288
- Hjorth, J., & Bloom, J. S. 2011, arXiv:1104.2274
- Hosokawa, T., Omukai, K., Yoshida, N., & Yorke, H. W. 2011, *Science*, 334, 1250
- Kalberla, P. M. W., Burton, W. B., Hartmann, D., et al. 2005, *A&A*, 440, 775
- Kashiyama, K., Nakauchi, D., Suwa, Y., Yajima, H., & Nakamura, T. 2013, *ApJ*, 770, 8
- Kawanaka, N., Piran, T., & Krolik, J. H. 2013, *ApJ*, 766, 31
- Kasen, D., & Woosley, S. E. 2009, *ApJ*, 703, 2205
- Klein, R. I., & Chevalier, R. A. 1978, *ApJ*, 223, L109
- Komissarov, S. S., & Barkov, M. V. 2010, *MNRAS*, 402, L25
- Kruehler, T., Tanvir, N. R., de Ugarte Postigo, A., et al. 2012, *GCN*, 13930, 1
- Kumar, P., Narayan, R., & Johnson, J. L. 2008, *MNRAS*, 388, 1729
- Levan, A. J., Tanvir, N. R., Starling, R. L. C., et al. 2013, arXiv:1302.2352
- MacFadyen, A. I., & Woosley, S. E. 1999, *ApJ*, 524, 262
- Matzner, C. D. 2003, *MNRAS*, 345, 575
- Matzner, C. D., & McKee, C. F. 1999, *ApJ*, 510, 379
- McKee, C. F., & Tan, J. C. 2008, *ApJ*, 681, 771
- Mészáros, P., & Rees, M. J. 2001, *ApJ*, 556, L37
- Mészáros, P., & Rees, M. J. 2010, *ApJ*, 715, 967
- Mészáros, P. 2013, *Astroparticle Physics*, 43, 134
- Mizuta, A., & Ioka, K. 2013, arXiv:1304.0163
- Morrison, R., & McCammon, D. 1983, *ApJ*, 270, 119
- Murase, K., & Ioka, K. 2013, arXiv:1306.2274
- Nagakura, H., Suwa, Y., & Ioka, K. 2012, *ApJ*, 754, 85
- Nakar, E., & Sari, R. 2012, *ApJ*, 747, 88
- Nakauchi, D., Suwa, Y., Sakamoto, T., Kashiyama, K., & Nakamura, T. 2012, *ApJ*, 759, 128
- Panaitescu, A., & Kumar, P. 2002, *ApJ*, 571, 779
- Pei, Y. C. 1992, *ApJ*, 395, 130
- Peng, F.-k., Hu, Y.-D., Xi, S.-Q., et al. 2013, arXiv:1302.4876
- Phinney, E. S. 1989, *The Center of the Galaxy*, 136, 543
- Popov, D. V. 1993, *ApJ*, 414, 712
- Quataert, E., & Kasen, D. 2012, *MNRAS*, 419, L1
- Rees, M. J. 1988, *Nature*, 333, 523
- Rhoads, J. E. 1997, *ApJ*, 487, L1
- Sari, R., Piran, T., & Narayan, R. 1998, *ApJ*, 497, L17
- Sari, R., Piran, T., & Halpern, J. P. 1999, *ApJ*, 519, L17
- Soderberg, A. M., Berger, E., Kasliwal, M., et al. 2006, *ApJ*, 650, 261
- Stratta, G., Gendre, B., Atteia, J. L., et al. 2013, arXiv:1306.1699
- Suwa, Y., & Ioka, K. 2011, *ApJ*, 726, 107
- Tan, J. C., & McKee, C. F. 2004, *ApJ*, 603, 383
- Thöne, C. C., de Ugarte Postigo, A., Fryer, C. L., et al. 2011, *Nature*, 480, 72
- Waxman, E., Mészáros, P., & Campana, S. 2007, *ApJ*, 667, 351
- Woosley, S. E. 1993, *ApJ*, 405, 273
- Woosley, S. E., Heger, A., & Weaver, T. A. 2002, *Reviews of Modern Physics*, 74, 1015
- Woosley, S. E., & Bloom, J. S. 2006, *ARA&A*, 44, 507
- Woosley, S. E., & Heger, A. 2012, *ApJ*, 752, 32
- Wu, X.-F., Hou, S.-J., & Lei, W.-H. 2013, *ApJ*, 767, L36
- Xu, D., de Ugarte Postigo, A., Leloudas, G., et al. 2013, arXiv:1305.6832
- Yonetoku, D., Murakami, T., Nakamura, T., et al. 2004, *ApJ*, 609, 935
- Zaninoni, E., Grazia Bernardini, M., Margutti, R., Oates, S., & Chincarini, G. 2013, arXiv:1303.6924
- Zhang, B., & Mészáros, P. 2001, *ApJ*, 552, L35
- Zhang, B., Fan, Y. Z., Dyks, J., et al. 2006, *ApJ*, 642, 354
- Zhang, B., Liang, E., Page, K. L., et al. 2007, *ApJ*, 655, 989
- Zhang, B.-B., Fan, Y.-Z., Shen, R.-F., et al. 2012, *ApJ*, 756, 190

## APPENDIX

### A. CALCULATION METHODS

In this appendix, we show the calculation method we use for evaluating electromagnetic emissions associated with BSG GRBs. Our method is based on the collapsar-jet scenario. Once a progenitor model and a set of phenomenological parameters are fixed, we can calculate physical quantities of the prompt emission, the afterglow emission, and the cocoon-fireball photospheric emission (CFPE) in a self-consistent manner.

#### A.1. Jet-cocoon Formation inside Progenitors

First, we model jet-cocoon formation within progenitors following our previous studies (Suwa & Ioka 2011; Nakauchi et al. 2012; Kashiyama et al. 2013). In this paper, we consider massive progenitors with  $M \gtrsim 40 M_{\odot}$ , which will collapse directly into a black hole (BH) without significant mass ejections (Heger et al. 2003). We assume that a bi-polar relativistic jet is launched when the mass of the central BH becomes  $3 M_{\odot}$ . The jet luminosity is proportional to the mass accretion rate onto the central BH,

$$L_j(t) = \eta_j \dot{M}(t) c^2. \quad (\text{A1})$$

This can be justified for jets driven by magneto-hydrodynamic mechanisms (e.g., Komissarov & Barkov 2010). Here,  $t$  is the time since the central engine becomes active in the GRB rest frame. The mass accretion rate  $\dot{M}(t)$  can be estimated as

$$\dot{M} = \alpha \frac{dM_r}{dt_{\text{ff}}(r)}, \quad (\text{A2})$$

where  $M_r$  is the mass coordinate, and  $\alpha$  represents the effect of disk accretion, which is set as  $\alpha = 1$  throughout this paper (Kumar et al. 2008).

The velocity of the jet head can be obtained from the pressure balance at the interface of the jet and the stellar envelope (Matzner 2003),

$$\beta_{\text{h}}(t) = \frac{\beta_j}{1 + \tilde{L}(t)^{-1/2}}, \quad (\text{A3})$$

$$\tilde{L}(t) = \frac{L_j(t - r_{\text{h}}/(\beta_j c))}{\Sigma_j(t) \rho_*(r_{\text{h}}) c^3},$$

where  $\beta_j \approx 1$  is the velocity of the jet and  $\rho_*(r)$  is the density of the stellar envelope. The radius of the jet head is obtained from  $r_h(t) = \int^t \beta_h(t')c dt'$  and  $\Sigma_j(t) = \pi r_h^2(t)\theta_j^2$  represents the cross section of the jet head where  $\theta_j$  is the jet opening angle. We regard that the jet breaks out the envelope when  $r_h(t_{\text{bo}}) = R_*$  where  $t_{\text{bo}}$  is the time of the jet break out. A successful GRB is expected if the central engine is still active after the breakout time, which corresponds to  $\dot{M}(t) \gtrsim 10^{-3}M_\odot \text{ s}^{-1}$  (e.g., Chen & Beloborodov 2007) at  $t > t_{\text{bo}}$  since the neutrino cooling is not effective for  $\dot{M}(t) < 10^{-3}M_\odot \text{ s}^{-1}$ . For BSG progenitors, we showed that jets can penetrate the progenitor envelopes irrespective of their masses (Suwa & Ioka 2011; Nakauchi et al. 2012; Kashiyama et al. 2013).

As far as the jet head is non-relativistic, i.e.,  $\beta_h \ll 1$ , shocked matter at the jet head will spread out sideways, and form a cocoon. The cocoon expands in the stellar envelope with a transverse velocity of

$$\beta_c(t) \sim \sqrt{\frac{E_c(t)}{3\rho_*(r_h)c^2V_c(t)}}, \quad (\text{A4})$$

which is obtained from the pressure balance at the interface of the cocoon and the stellar envelope (Matzner 2003)<sup>11</sup>. We assume that the cocoon has a conical shape with a height of  $r_h(t)$  and a circular radius of  $r_c(t) = \int^t \beta_c(t')c dt'$  at the bottom. Then, the volume of the cocoon  $V_c$  can be estimated as  $V_c(t) = \pi r_c(t)^2 r_h(t)/3$ . As it expands, cocoon also loads the stellar material along the direction of motion and the mass loaded in the cocoon can be evaluated from

$$M_c(t) = \frac{r_c(t)^2}{4r_h(t)^2} \int^{r_h(t)} 4\pi r^2 \rho_*(r) dr. \quad (\text{A5})$$

Before the jet breakout, most of the jet energy is stored in the cocoon and the cocoon energy can be described as  $E_c(t) = \int^t L_j(t' - r_h/c) dt'$ .

In summary, we can calculate the jet breakout time  $t_{\text{bo}}$ , the cocoon energy  $E_c(t_{\text{bo}})$  and the mass of the cocoon  $M_c(t_{\text{bo}})$  by fixing the progenitor model and the central engine parameters ( $\theta_j, \eta_j$ ). In this paper, we assume that both  $\eta_j$  and  $\theta_j$  are constants for simplicity (but see e.g., Kawanaka et al. 2013; Mizuta & Ioka 2013).

### A.2. Prompt Emission

After the jet breakout, a fraction of the jet energy will be dissipated and radiated as prompt gamma-rays. Since the mechanism is still highly uncertain, we here do not discuss the energy spectrum (see Nakauchi et al. 2012, for discussion about the spectrum of prompt emissions). Instead, we estimate the isotropic energy  $E_{\gamma,\text{iso}}$  and the prompt duration  $\delta t_\gamma$ , and compare them with the observed ones.

In general, the dissipation radius is larger than the progenitor radius, and the prompt emission starts at  $t \sim t_{\text{bo}}$ . Following the results of e.g., Chen & Beloborodov (2007), we suppose that the prompt emission ends when the mass accretion rate becomes smaller than the critical value  $\dot{M}(t_{\text{fin}}) \sim 10^{-3} M_\odot \text{ s}^{-1}$ . Hence, one can evaluate the duration of the prompt emission as

$$\delta t_\gamma = (t_{\text{fin}} - t_{\text{bo}})(1 + z), \quad (\text{A6})$$

and the isotropic energy as

$$E_{\gamma,\text{iso}} = \int_{t_{\text{bo}}}^{t_{\text{fin}}} L_{\text{iso}}(t') dt', \quad (\text{A7})$$

where  $L_{\text{iso}}(t) = \epsilon_\gamma(4/\theta_j^2)L_j(t)$  is the isotropic luminosity of the prompt emission, and  $\epsilon_\gamma$  is the radiation efficiency.

In summary, we fix  $(\theta_j, \eta_j, \epsilon_\gamma)$  to reproduce  $E_{\gamma,\text{iso}}^{\text{obs}}$  and  $\delta t_\gamma^{\text{obs}}$  of ULGRBs. These parameters have been inferred for LGRBs both observationally and theoretically. The typical value of  $\theta_j$  is estimated as  $\theta_j \sim 5^\circ$  for bursts with jet-break signature in the afterglow light curve (Ghirlanda et al. 2004; Soderberg et al. 2006). From the prompt and afterglow observations,  $\epsilon_\gamma$  is estimated as  $\epsilon_\gamma \sim 0.01$ -1 (Zhang et al. 2007). The observed LGRBs typically have  $E_{\gamma,\text{iso}}^{\text{obs}} \sim 10^{52}$ - $10^{54}$  erg and  $\delta t_\gamma^{\text{obs}} \sim 10$ -100 s. Suwa & Ioka (2011) argued that these typical features of LGRBs can be reproduced for a WR progenitor, if we apply our prescription, setting  $\theta_j \sim 5^\circ$ ,  $\epsilon_\gamma \sim 0.01$ -1, and  $\eta_j = 6.2 \times 10^{-4}$ . Kawanaka et al. (2013) theoretically estimated the jet efficiency as  $\eta_j \sim 10^{-4}$ - $10^{-3}$ . In this paper, we take  $\eta_j = 6.2 \times 10^{-4}$  as a fiducial value, and change its value as  $\eta_j \sim 10^{-4}$ - $10^{-3}$  for fitting.

### A.3. Afterglow Emission

We calculate the afterglow emissions based on the standard external shock model (Sari et al. 1998). The relativistic jet finally decelerates in the interstellar medium, where a fraction of electrons is accelerated to relativistic energies at the forward shock, and emits synchrotron radiation in magnetic fields amplified by the shock. For the observed ULGRBs, the normal decay phase of the afterglow starts at  $t_{\text{obs}} \sim 10^5$  s, which corresponds to the slow cooling phase,

<sup>11</sup> Matzner (2003) represents the cocoon pressure as  $P_c \sim E_c/3\rho_*V_c$ , which is a typo. Correctly, it should be  $P_c \sim E_c/3V_c$ .

and the jet break is not confirmed until  $\sim 2 \times 10^6$  s (Levan et al. 2013). If we follow Eqs. (8) and (11) in Sari et al. (1998), the light curves can be modeled as

$$F_\nu \sim \begin{cases} 0.061 f(p)^{p-1} \epsilon_{e,-1}^{p-1} \epsilon_{B,-2}^{\frac{p+1}{4}} E_{\text{kin},53}^{\frac{p+3}{4}} n^{1/2} D_{28}^{-2} (1+z)^{\frac{3-p}{2}} t_4^{-\frac{3p-3}{4}} \left(\frac{\nu}{10^{14} \text{ Hz}}\right)^{\frac{1-p}{2}} \text{ Jy} & (\nu_m < \nu < \nu_c), \\ 9.8 \times 10^{-4} f(p)^{p-1} \epsilon_{e,-1}^{p-1} \epsilon_{B,-2}^{\frac{p-2}{4}} E_{\text{kin},53}^{\frac{p+2}{4}} n^0 D_{28}^{-2} (1+z)^{\frac{2-p}{2}} t_4^{-\frac{3p-2}{4}} \left(\frac{\nu}{10^{16} \text{ Hz}}\right)^{-\frac{p}{2}} \text{ Jy} & (\nu_c < \nu), \end{cases} \quad (\text{A8})$$

with the characteristic frequency and the cooling frequency of synchrotron radiation

$$\nu_m \sim 4.6 \times 10^{13} f(p)^2 \epsilon_{e,-1}^2 \epsilon_{B,-2}^{1/2} E_{\text{kin},53}^{1/2} (1+z)^{-1} t_4^{-3/2} \text{ Hz}, \quad (\text{A9})$$

and

$$\nu_c \sim 2.6 \times 10^{15} \epsilon_{B,-2}^{-3/2} E_{\text{kin},53}^{-1/2} n^{-1} (1+z)^{-1} t_4^{-1/2} \text{ Hz}, \quad (\text{A10})$$

where we use  $Q_x = Q/10^x$  in CGS units, and  $\nu$  is the observed photon frequency. Here,  $p$  is the power law index of the non-thermal electrons,  $f(p) = 3(p-2)/(p-1)$ ,  $\epsilon_e$  is the electron-acceleration efficiency,  $\epsilon_B$  is the amplification efficiency of magnetic field, and  $n$  is the ambient matter density.  $D$  and  $z$  are the luminosity distance and the red shift of the source, respectively. Using  $E_{\gamma,\text{iso}}$  and  $\epsilon_\gamma$  introduced in §A.2, the kinetic energy of the relativistic ejecta is calculated as  $E_{\text{kin}} = E_{\gamma,\text{iso}}(1 - \epsilon_\gamma)/\epsilon_\gamma$ .

In X-ray and UV/optical/IR bands, the extinction both in the Milky Way (MW) and the host galaxy is important. For X-ray absorption, we use the cross section of the photoelectric absorption per HI atom shown in Morrison & McCammon (1983), assuming solar abundance. The measured HI column density of the MW is  $N_{\text{H}}^{\text{MW}} = 1.5 \times 10^{20} \text{ cm}^{-2}$  (Kalberla et al. 2005). The HI column densities of the host galaxies are measured as  $N_{\text{H}}^{\text{host}} = 1.2 \times 10^{21} \text{ cm}^{-2}$  for GRB 101225 (Levan et al. 2013),  $N_{\text{H}}^{\text{host}} = 1.9 \times 10^{21} \text{ cm}^{-2}$  for GRB 111209 (Levan et al. 2013), and  $N_{\text{H}}^{\text{host}} = 1.3 \times 10^{22} \text{ cm}^{-2}$  for GRB 121027 (Peng et al. 2013), respectively. In UV/optical/IR bands, we refer the MW extinction for each burst to Levan et al. (2013). The host extinction in each band can be calculated from the formula

$$A_\lambda^{\text{host}} = \xi(\lambda) \left(1 + \frac{1}{R_V}\right) A_V^{\text{host}}, \quad (\text{A11})$$

where  $\xi(\lambda) \equiv A_\lambda^{\text{host}}/A_B^{\text{host}}$ , and  $R_V \equiv A_V^{\text{host}}/E_{B-V}$  is the ratio of total-to-selective extinction. Three types of extinction curves are studied in Pei (1992) for the MW, Large Magellanic Cloud, and Small Magellanic Cloud (SMC), and they are used in evaluating the extinction of other galaxies with the parameter,  $A_V^{\text{host}}$ . We apply the SMC type extinction law for ULGRB host, since they are blue compact galaxies. We refer the fitting formula of  $\xi(\lambda)$  to Eq. (20) and Table 4 in Pei (1992), and the value of  $R_V = 2.93$  to Table 2 in Pei (1992). Thus, extinctions are parameterized only by  $A_V^{\text{host}}$ .

In summary, we additionally introduce 5 parameters ( $p, \epsilon_e, \epsilon_B, n, A_V^{\text{host}}$ ) to fit the standard afterglow component in XRT (0.3-10 keV) and UV/optical/IR bands. Practically, there are 4 constraints on these parameters from the observations. For some GRBs, the range of 4 parameter ( $p, \epsilon_e, \epsilon_B, n$ ) values are obtained from the afterglow observations as  $p \sim 1.4-2.8$ ,  $\epsilon_e \sim 4 \times 10^{-3}-0.1$ ,  $\epsilon_B \sim 4 \times 10^{-5}-0.07$ , and  $n \sim 0.01-100 \text{ cm}^{-3}$ , respectively (e.g., Panaitescu & Kumar 2002). From observation, the V-band extinction takes values of  $A_V^{\text{host}} \sim 0.1-3.0$  (Covino et al. 2013; Zaninoni et al. 2013).

#### A.4. Cocoon-Fireball Photospheric Emission

When jets penetrate the progenitors, hot-plasma cocoons also come out. Such cocoons are radiation-dominated and non-relativistic, i.e.,  $E_c(t_{\text{bo}})/M_c(t_{\text{bo}})c^2 < 1$  (Kashiyama et al. 2013). They first expand almost adiabatically, and then emit quasi-thermal photons from the photosphere, where the Thomson optical depth  $\tau_T$  becomes unity. Since cocoon fireballs would load hydrogens from BSG envelopes, these processes are quite similar to those of shock-heated ejecta responsible for Type IIP SNe, which have been well modeled (Arnett 1980; Popov 1993; Kasen & Woosley 2009). Here, we calculate CFPEs following Arnett (1980) and Popov (1993).

Arnett (1980) and Popov (1993) analytically formulated photospheric emissions from spherically expanding shock-heated ejecta. There are 4 input parameters; the initial ejecta radius  $R_0$ , the internal energy  $E \equiv E_c(t_{\text{bo}})$ , the baryon mass  $M \equiv M_c(t_{\text{bo}})$ , and the expansion velocity scale  $v_{\text{sc}}$ . Here, we set the initial conditions for cocoon fireballs at  $R_0 \sim 2R_*$ , where roughly a half the internal energy is transferred to the kinetic energy and cocoon fireballs become almost spherical;

$$E_{\text{th},0} = E/2, \quad (\text{A12})$$

$$v_{\text{sc}} = \sqrt{10E/3M}. \quad (\text{A13})$$

Beyond the saturation radius,  $R(t) \sim v_{\text{sc}} \times t > R_0$ , we consider a homologous expansion of cocoon fireballs (Arnett 1980; Popov 1993);

$$r = x \times R(t), \quad (\text{A14})$$

$$v(r, t) = x \times v_{sc}. \quad (\text{A15})$$

We assume uniform densities of  $\rho(t) = \rho_0(R(t)/R_0)^{-3}$  with  $\rho_0 = 3M/4\pi R_0^3$ . The temperature structure inside the fireball,  $T(r, t)$ , can be obtained by solving the equation below;

$$\frac{\partial e}{\partial t} + P \frac{\partial}{\partial t} \left( \frac{1}{\rho} \right) = - \frac{\partial L}{\partial m_r}, \quad (\text{A16})$$

where  $e(t) = aT^4(t)/\rho(t)$  is the specific internal energy,  $P(t) = aT^4(t)/3$  is the radiation pressure,  $L = -(4\pi r^2 ac/3\kappa_T \rho) \times \partial T^4/\partial r$  represents the radiative energy loss,  $m_r$  is the mass coordinate, and  $a = 7.56 \times 10^{-15} \text{ erg cm}^{-3} \text{ K}^{-4}$  is the radiation constant. For the opacity of cocoon fireballs,  $\kappa$ , we simply assume a step function;

$$\kappa = \begin{cases} \kappa_T = 0.34 \text{ cm}^2 \text{ g}^{-1} & T > T_{\text{ion}}, \\ 0 & T < T_{\text{ion}}. \end{cases} \quad (\text{A17})$$

Here,  $\kappa_T$  is the Thomson opacity, and  $T_{\text{ion}} \approx 6000 \text{ K}$  is the hydrogen recombination temperature in the cocoon fireball. For  $T < T_{\text{ion}}$ , the recombination of hydrogen atoms occurs and the opacity becomes effectively zero.

Arnett (1980) and Popov (1993) solved Eq. (A16) with Eq. (A17) where the photosphere radius evolves as

$$R_{\text{ph}}(t) \sim \begin{cases} R(t), & (t_e \ll t < t_i), \\ R_{\text{ion}}(t), & (t_i < t). \end{cases} \quad (\text{A18})$$

Here,  $t_e = R_0/v_{sc}$ , and  $t_i$  corresponds to the time at which the effective temperature of the photosphere becomes equal to the hydrogen recombination temperature  $T_{\text{ion}} \approx 6000 \text{ K}$  as shown below. Afterward it, the recombination front appears in the cocoon fireball. The recombination front,  $R_{\text{ion}}(t)$ , evolves as

$$R_{\text{ion}}(t)^2 = v_{sc}^2 \left[ t_i t \left( 1 + \frac{t_i^2}{3t_a^2} \right) - \frac{t^4}{3t_a^2} \right]. \quad (\text{A19})$$

with  $t_a = \sqrt{2t_d t_e}$  and the photon diffusion time  $t_d \equiv 9\kappa_T M/(4\pi^3 c R_0)$ . The bolometric luminosity of the photospheric emission is described as

$$L(t) = \begin{cases} (E_{\text{th},0}/t_d) \exp(-t^2/t_a^2), & (t_e \ll t < t_i), \\ 4\pi R_{\text{ion}}(t)^2 \sigma_{\text{SB}} T_{\text{ion}}^4 & (t_i < t), \end{cases} \quad (\text{A20})$$

which gives the effective temperature of the photosphere as

$$T_{\text{eff}}(t) = \begin{cases} T_{\text{eff}}(0) \exp(-t^2/4t_a^2) (t_e/t)^{1/2}, & (t_e \ll t < t_i), \\ T_{\text{ion}} & (t_i < t). \end{cases} \quad (\text{A21})$$

Here,  $T_{\text{eff}}^4(0) \equiv E_{\text{th},0}/(4\pi R_0^2 \sigma_{\text{SB}} t_d)$  and  $\sigma_{\text{SB}}$  is the Stefan-Boltzmann constant. The transition time  $t_i$  can be iteratively determined from the condition  $T_{\text{eff}}(t_i) = T_{\text{ion}}$ .

Now that the evolution of the photospheric radius and its temperature is determined, one can calculate the CFPE as

$$F_{\lambda_{\text{obs}}}(t) d\lambda_{\text{obs}} = \pi B_{\lambda}(T_{\text{eff}}(t)) d\lambda \frac{R_{\text{ph}}(t)^2}{D^2}, \quad (\text{A22})$$

where  $B_{\lambda}(T) = 2hc^2/\lambda^5(\exp(hc/\lambda k_B T) - 1)^{-1}$ ,  $h$  is the Planck constant and  $k_B$  is the Boltzmann constant.